
2D and 3D Numerical Simulations of TIG Welding of a 316L Steel Sheet

Lionel Depradeux — Jean-François Jullien

INSA de Lyon

20 Avenue Albert Einstein

F-69621 Villeurbanne cedex

lionel.depradeux@insa-lyon.fr, jean-francois.jullien@insa-lyon.fr

ABSTRACT. In this study, a numerical simulation to predict residual stresses and distortion generated by a TIG welding process is presented. 3D numerical simulations have been performed on an instrumented test involving a fusion line along the long axis direction of a 316L plate. For the transient thermal analysis, the heat-input modeling was calibrated against thermocouple measurements. The subsequent mechanical analysis was performed with elasto-viscoplastic (EVP) or elasto-plastic (EP) constitutive equations, in order to investigate viscosity effects. Both results of EP and EVP calculations have been compared to the experimental results (transient displacements, final shape, and residual stresses). Afterward, the relevance of a simplified 2D-plane stress modeling of this test case, for the prediction of residual stresses, is discussed.

RÉSUMÉ. Dans cette étude, nous présentons une simulation numérique en vue de la prédiction des distorsions et contraintes résiduelles générées par une opération de soudage TIG. Des simulations 3D d'un test de soudage instrumenté, impliquant la création d'une ligne de fusion le long de l'axe central d'une plaque en acier 316L, ont été réalisées. Pour l'analyse thermique transitoire, la modélisation de l'apport de chaleur a été calée sur des mesures de températures par thermocouples. Après quoi, l'analyse mécanique a été effectuée avec une loi de comportement élasto-viscoplastique d'une part, et élasto-plastique d'autre part, de façon à étudier l'influence de la viscosité. Les résultats de simulations (EP et EVP) ont été comparés aux résultats expérimentaux (déplacements transitoires, déformée finale, contraintes résiduelles). Après quoi la pertinence d'une modélisation simplifiée 2D en contraintes planes de cet essai, pour la prédiction des contraintes résiduelles, est discutée.

KEYWORDS: finite element analysis, welding, TIG, 2D welding simulation, 3D welding simulation, austenitic stainless steel.

MOTS-CLÉS : éléments finis, soudage TIG, simulation 2D, simulation 3D, acier inoxydable austénitique.

1. Introduction

During a TIG welding operation, the non-uniform heat supplied and the subsequent cooling generate distortions and residual stresses. Whereas distortions can cause tolerances problems, residual stresses can be a source of cracking and fractures problems in welded structures, such as welded pipes in boiling-reactor piping systems of nuclear power plants, made of austenitic stainless steel. With the recent increasing of computer power, numerical simulation by the finite element method has become a highly effective mean of estimating transient stresses, residual stresses and distortions generated by the welding process.

However, accurate prediction of residual stresses and distortions remain very difficult since the welding process involves very complex thermal, metallurgical and mechanical phenomena in the Heat Affected Zone. Given the complexity of this coupled problem, it is therefore usual to neglect some physical aspects, or to reduce the dimension of the problem in order to enable less time-demanding simulations. Therefore, the complete three-dimensional problem is currently reduced to one of plane strain or plane stress.

In this study, we focus on the thermo-mechanical behavior of AISI 316L stainless steel, during a TIG welding process. The aim of the study is to assess the ability of the numerical simulation to predict transient displacements, residual stresses, and distortions, for a simplified test representative of a welding operation. The sensitivity of the numerical results to the constitutive equation is also investigated. Therefore, a parallel experimental and numerical study is carried out on a test that considers the creation of a fusion line along the center of a 316L plate, using the TIG welding technique, without filler material. A large quantity of measurements is provided during the test (temperatures, displacements) and after the cooling stage (final shape, residual stresses).

Different kinds of modeling of this test case are considered in this study. In order to capture the transient thermal and deformation history accurately enough, a complete three-dimensional simulation of this test is firstly performed, taking into account time-dependant plasticity for high temperatures, by the use of an elasto-viscoplastic constitutive equation. Secondly, the results are compared to the solution given by three-dimensional simulations assuming non time-dependant plasticity, considering isotropic or kinematic hardening. All the numerical results are also compared to experimental results.

Lastly, we investigate for this test the relevance of a two-dimensional simulation, assuming a plane stress hypothesis, for the prediction of the residual stresses. The results of the 2D simulations are compared to the experiment, and to the results of the 3D simulations.

All the simulations in this study are performed with the finite element code *Code_Aster*, developed by Electricité de France.

2. Material and experimental procedure

2.1. Material

The testing specimens are made of AISI 316L stainless steel. This steel is widely used in nuclear industry, for its good resistance when submitted to thermal and mechanical solicitations. It is entirely austenitic from room temperature to its temperature of fusion, by virtue of its high nickel content. Therefore, there is no metallurgical transformation occurring in the solid part of the Heat Affected Zone during welding. The chemical composition of the steel is given in table 1.

Comp.	C	Si	Mn	P	S	Cr	Ni	Mo	N
316L	0,024	0,38	1,76	0,023	0,001	17,31	12,05	2,55	0,07

Table 1. *Chemical composition of the steel*

2.2. Welding procedure

The specimen chosen for the experiment is a plate (260×160×10 mm³, see fig. 1). A single pass weld is created along the center of the sheet in the long axis direction. The TIG welding technique, without filler material, is considered. The weld begins and ends 10mm from the plate edges. The welding parameters used for the trial are tension $U = 10V$, intensity $I = 150A$, and a travelling speed of $1 \text{ mm}\cdot\text{s}^{-1}$. The plate is lying on three points in its lower face, without other mechanical loading. The temperature gradients in the vicinity of the weld line during the heating and cooling stage, and the local decrease of mechanical properties at high temperatures yield to non-homogeneous residual stresses and permanent distortions after the process.

2.3. Measurements performed

Two types of measurement are performed continuously during the welding. On the one hand, temperatures are continuously recorded in two sections perpendicular to the welding direction, using K type thermocouples (78 microns diameter), positioned every two millimeters in the lower face, and in some points in the upper face. Fig. 2 shows the evolution of transient temperatures for both sections orthogonal to the welding direction. The hypothesis of steady state can be assumed from the thermal point of view.

On the other hand, 8 LVDT sensors (C5 to C6), as shown in fig. 1, measure transient vertical displacements. Sensors C1 to C5 provide the displacement under the fusion line, and 12mm from the center. The sensor C6 is positioned to verify that

the symmetry is being conserved. Welding parameters (Tension, Intensity, travelling speed of the torch) are also continuously recorded during the test.

After cooling, the final shape of both sides (upper and lower face) of the plate is measured, for a cross-section perpendicular to the welding direction. Longitudinal and transverse residual stresses are also evaluated by an X-Ray diffraction technique, in the lower face of the specimen, for a cross-section located at $X = 150$ mm.

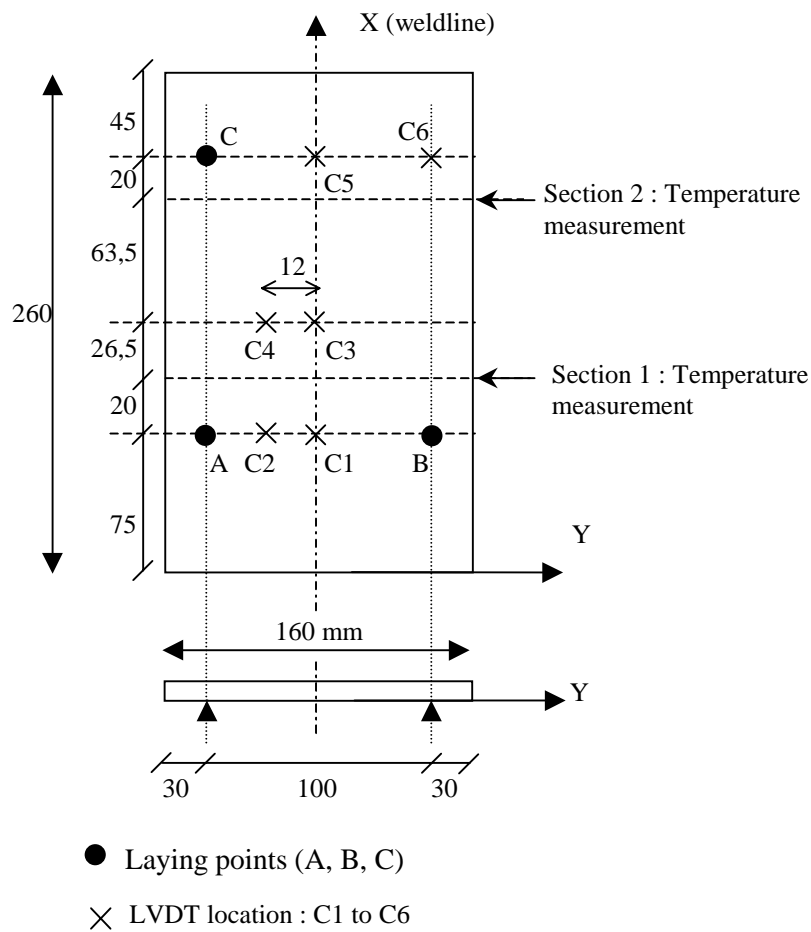


Figure 1. *Experimental device and sensors location*

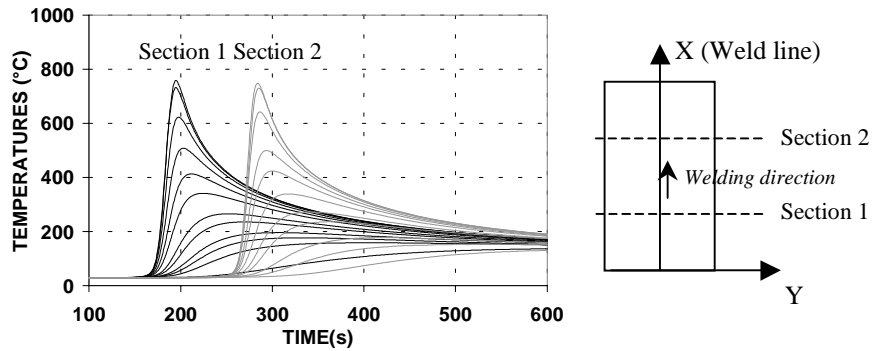


Figure 2. Temperature evolution measured by thermocouples in two cross-sections, orthogonal to the welding direction

3. Three-Dimensional finite element simulation

3.1. Thermal analysis

An uncoupled thermo-mechanical analysis is considered in this study. The thermal analysis is performed at first, during which the time-dependent temperature field is saved for the subsequent mechanical analysis (stresses, displacements).

Due to the symmetry of the plate, only one half is modeled, using quadratic three-dimensional prismatic volume elements. 5 quadratic elements are set through the thickness. A dense mesh is used in the vicinity of the weld line, and a coarser mesh for the rest of the structure. The final mesh, with approximately 10 000 nodes, is the result of a compromise between computing time and accuracy (fig. 4).

The thermal analysis is performed in two steps. Firstly, the quasi-steady-state technique is used for the thermal solution, in order to adjust faster the heat source parameters against temperature measurements. The quasi-steady-state technique assumes a non time-dependant temperature field in the heat source co-moving frame (see for instance Shanghvi *et al.*, 2002). The heat conduction equation writes, in an eulerian frame moving with the heat source:

$$-\vec{V} \cdot \text{grad}H - \text{div}(\lambda \cdot \text{grad}T) = G \quad [1]$$

Where V is the heat source velocity, H the enthalpy of the material, λ the thermal conductivity, and G an eventual internal body heat source. All the thermo-physical characteristics are considered temperature-dependent (see fig. 3), and the effect of latent heat of fusion is taken into account, by using the enthalpy method. A latent

heat of fusion of 1800 MJ.m^{-3} is adopted, between the solidus and liquidus temperatures, respectively $T_s = 1450^\circ\text{C}$ and $T_f = 1500^\circ\text{C}$. A larger value of the thermal conductivity is classically introduced for temperatures exceeding the melting temperature, in order to homogenize the temperature field in the melted zone (Lindgren, 2001). The thermal conductivity has therefore been doubled for temperatures exceeding T_f , as it is currently assumed (see for instance Brickstad, 1997).

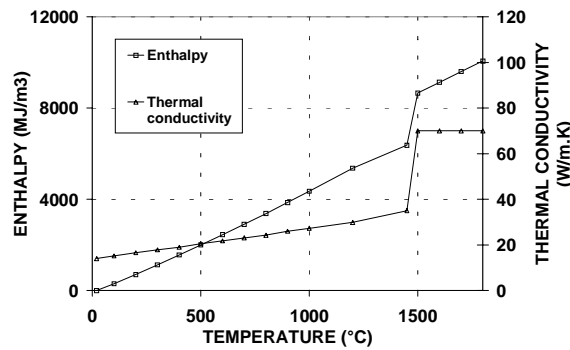


Figure 3. Evolution of thermal properties (thermal conductivity and enthalpy) with temperature

For the heat source modeling, no attempt is made to model the physics of the arc process, or thermo-fluids phenomena that take place in the weld pool. We only consider a total net heat input, which incorporates the efficiency η of the arc, assuming a spatial distribution of this heat input. This spatial distribution can be represented by different kinds of mathematical models, from the simple point source of Rosenthal (Rosenthal, 1941), to the double ellipsoid proposed by Goldak (Goldak *et al.*, 1984). Given that the welding does not involve filler material, and that the weld pool depth is rather small, the chosen heat source presents a surface heat flux density, with a triangular aspect (fig.4). The efficiency parameter η is chosen so as to adjust the simulated temperatures with the measured ones on the lower face of the plate.

We consider no heat exchange on the plane of symmetry (adiabatic thermal boundary conditions), and for other faces, radiative and convective thermal exchanges with the environment with a convective coefficient $h = 5 \text{ W.}^\circ\text{m}^{-2}\text{C}^{-1}$ and an emissivity $\varepsilon = 0,75$ with ω the Stefan-Boltzmann constant, in the equation :

$$-\lambda \frac{\partial T}{\partial n} = h(T - T_{air}) + \varepsilon \omega (T^4 - T_{air}^4) \quad [2]$$

After calibration of the heat source, we found 65% for the heat-input efficiency of the arc, in accordance with classical efficiency values for the TIG process. This final heat source modeling is then used at second step for the non-stationary thermal analysis, which considers the whole thermal cycle, from the beginning of the heating to the end of the cooling. The heat conduction equation writes, for the complete transient thermal analysis:

$$\frac{\partial H}{\partial t} - \text{div}(\lambda \cdot \text{grad}T) = G \quad [3]$$

In this case, the triangular heat source is moving along the axis of the plate, with convective and radiative exchanges at the surface of the specimen, with the same emissivity and convective coefficient used for the steady-state analysis.

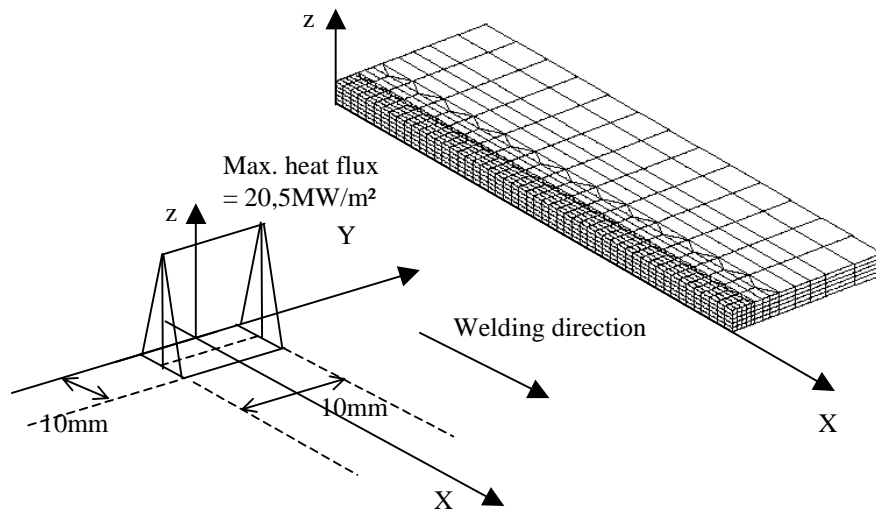


Figure 4. Heat source modelling and mesh used for the 3D model

3.2. Mechanical analysis

After the thermal simulation, the time-dependent temperature field is used for the mechanical analysis. Two kinds of modeling are considered.

3.2.1. Elastoviscoplastic (EVP) computation

At first, in order to take into account rate-dependent plasticity at high temperature, an elasto-viscoplastic calculation is performed. The material is

assumed to be elasto-plastic for low temperatures (non rate-dependant), and elasto-viscoplastic for high temperature.

The EVP constitutive equation, implanted in the FE code, is dedicated to welding processes and heat treatments. The three dimensional formulation of the viscoplastic strain rate writes:

$$f(\sigma, r, T) = \sigma^{VM} - R(r, T) - \sigma_s \leq 0 \quad [4]$$

$$\dot{\epsilon}_{ij}^{vp} = \frac{3}{2} \dot{p} \frac{S_{ij}}{\sigma^{VM}} \quad \text{and} \quad \dot{p} = \left(\frac{\langle \sigma^{VM} - R(r) - \sigma_s \rangle}{\mu} \right)^n \quad [5], [6]$$

$$\begin{cases} R = R_0 r \\ \dot{r} = \dot{p} - (Cr)^m \end{cases} \quad [7]$$

Where σ^{VM} is the von Mises effective stress, σ_s the yield of viscoplastic flow, R_0 the modulus of linear hardening, and μ and n two coefficients of viscosity. This model considers an elastic domain that evolves with an additive isotropic hardening, with a term of viscous recovery in which appear the parameters C and m . All viscous parameters are temperature-dependent. At low temperatures, the elasto-plastic behaviour is described by writing equation 4:

At low temperature a purely elasto-plastic behaviour is considered, μ is set to zero, then \dot{p} can only be determined by the consistency condition, corresponding to the non-rate dependent plasticity.

For very high temperatures ($T > 1450^\circ\text{C}$), the model degenerates into a Newtonian fluid type, assuming a complete recovery of hardening ($C = m = 1$ in equation 7).

3.2.2. Elastoplastic (EP) computation

It is for common use to neglect viscous effects when simulations of welding are performed, mainly because viscous parameters are difficult to obtain (Lindgren, 2001). As a consequence, purely elasto-plastic, bi-linear models are usually entered in the Finite Element model. For that reason, purely elasto-plastic simulations are also performed for our test case, in order to investigate the importance of viscous effects. The Von Mises plasticity with linear hardening is considered, assuming on the one hand isotropic hardening (isotropic enlargement of the yield function), and on the other hand, kinematic hardening (translation of the yield function). Kinematic hardening is supposed to be more adapted in case of cyclic loading, as it can partially take into account Bauschinger effect. Since the material in the vicinity of

the weld is subjected to reversed plastic yielding during the cooling phase, the influence of isotropic or kinematic assumption for the hardening would be brought out in this region.

3.2.3. Mechanical data

All requisite material data including their temperature dependency are entered in the FE model. Material data (elasto-plastic and elasto-viscoplastic) have been deduced from a complete thermo-mechanical characterization of the steel, performed in our laboratory. Dilatation tests provided expansion coefficient, and traction tests at various temperatures and with two deformation rates ($0,25\%.s^{-1}$ and $0,025\%.s^{-1}$) have been realized in order to obtain elasto-plastic data, that is: Young's modulus, yield stress, linear hardening's modulus (see figs 5 and 6.).

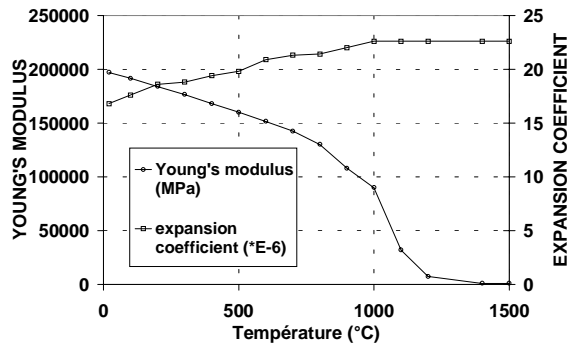


Figure 5. Evolution of Young's modulus and expansion coefficient ($\times 10^{-6} K^{-1}$) with the temperature

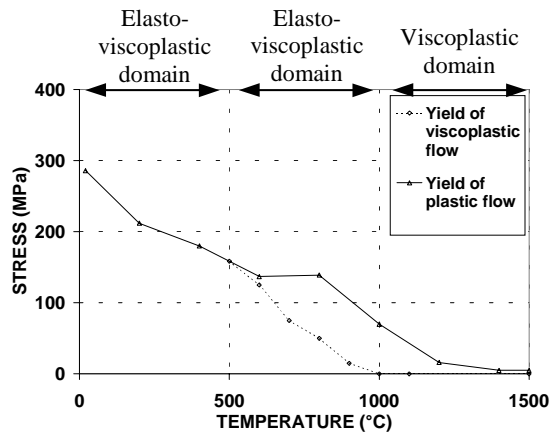


Figure 6. Evolution of plastic and viscoplastic yield stress with the temperature

Viscoplastic data have been deduced from creep and relaxation tests above 500°C, as viscosity effect is not taken into account below this temperature ($\eta = 0$ for $T < 500^\circ\text{C}$ in eq. 8). The yield of viscoplastic flow is set to zero for $T > 1000^\circ\text{C}$ (fig. 6), the behaviour is then purely viscoplastic above this temperature, in the case of the EVP simulation.

We assumed that the expansion coefficient was constant for temperatures exceeding the melting temperature, and so we did for elasto-plastic data above the melting temperature, in the case of EP simulation. As a matter of fact no further changes in the material properties are accounted for in the mechanical analysis for temperature exceeding T_f . For temperatures exceeding T_f , the yield stress and the Young's modulus are consequently set to low values, but not zero because a too soft weld metal may give numerical problems in the model. The Young's modulus, for instance, is set to a value equal to 5% its value at room temperature, for $T > T_f$.

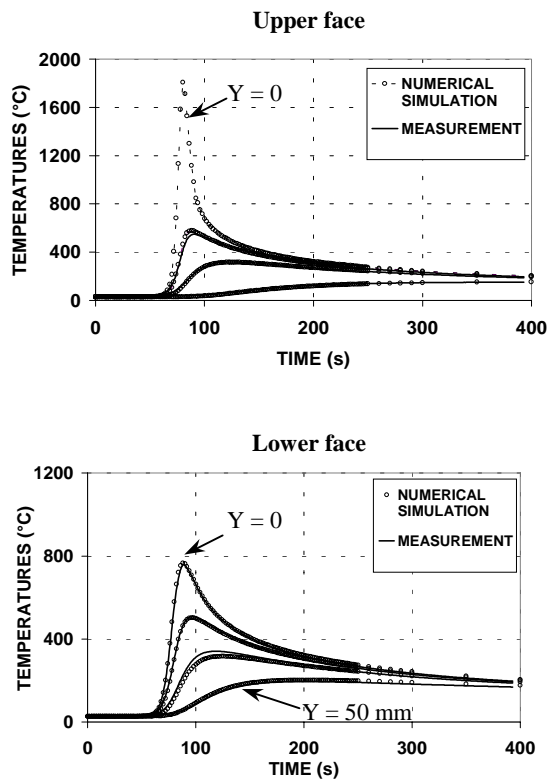


Figure 7. Comparison between calculated and measured temperatures in the upper and the lower face of the plate, for a cross-section

3.3. Results of the 3D analysis - Temperatures

Fig. 7 compares the evolution of measured and calculated temperatures, for the transient analysis. The temperatures measured in the lower face were used to calibrate the heat input modeling, and that explains the very good agreement of the simulation with the experimental results. In the upper face, for which temperature measurements were not used to calibrate the heat source, there is however also a good agreement between simulation and measurements, up to 10mm from the weld centerline. No temperature measurement was possible closer to the fusion line, but the comparison between the calculated weld pool and a picture of the melted zone (fig. 8) shows a very good agreement, and validates the heat source modeling.

The 3D model allows us to reproduce very well the temperature evolution in the specimen during the welding, but also during the cooling stage. Heat losses seem to be correctly taken into account by the radiative and convective coefficients.

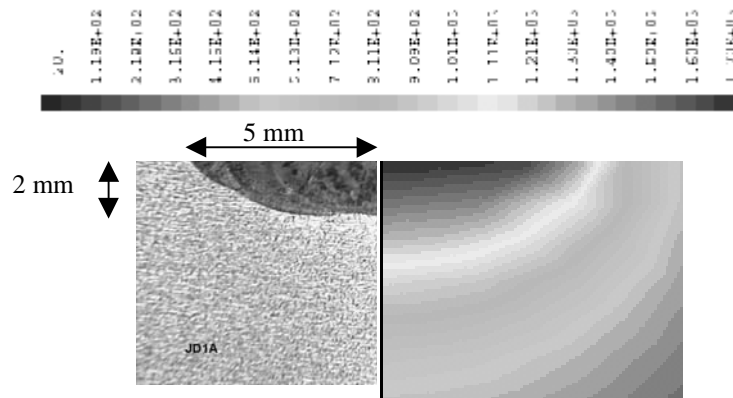


Figure 8. Calculated temperature distribution during the welding in a cross section, and comparison with a picture of the melted zone

3.4. Results of the 3D analysis - Vertical displacements and final shape

3.4.1. EVP simulation

The evolutions of the vertical displacements measured by sensors C1 to C6 are shown on fig. 9. The center of the plate is going down as the heat source passes along the axis of the plate. A 3D effect is observed: the sensor C3 measures a higher maximal deflection than the sensor C1 during the passage of the heat source, whereas the center of gravity of the plate is elevating after the heat source passage and during the cooling stage. The measured displacement of sensor C6 shows that

the symmetry is being very good conserved during the welding, but less during the cooling stage.

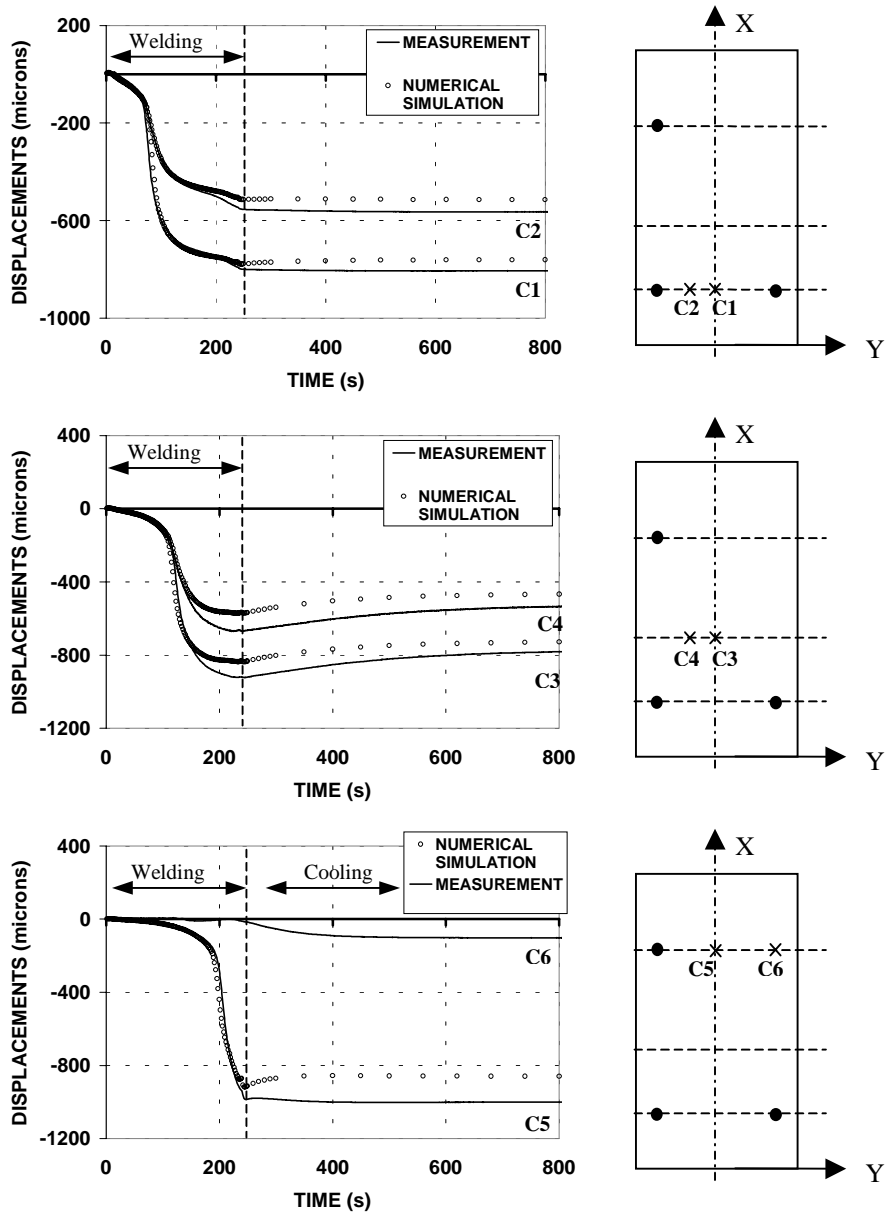


Figure 9. Evolution of transient vertical displacements (sensors C1 to C6) during the test: comparison between EVP numerical simulation and measurements

The comparison between the calculated transient vertical displacements and the experimental ones is very satisfactory if considering also experimental error (around more or less 10 microns). The global effect of bending of the plate is very well reproduced during the path of the heat source, but also during the cooling stage in the first section where the symmetry is better conserved. Moreover, the three-dimensional effect, which results in flexion in both the longitudinal and the transversal direction, is well reproduced.

The main distortion observed after the cooling is a deflection of the center in the transverse direction. Fig. 10 compares experimental and numerical results for the final shape of the plate, considering the section situated at the level of the first line of support. It also indicates a very good agreement.

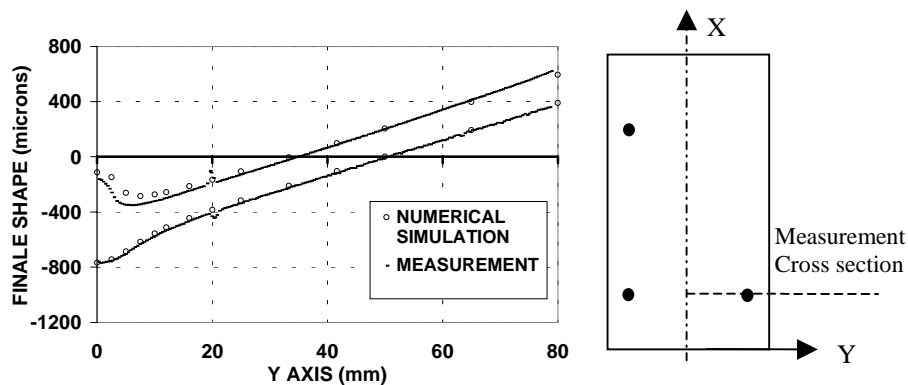


Figure 10. Final shape of a half cross-section: comparison between EVP numerical simulation and measurements

3.4.2. Comparison with EP simulation

Fig. 11 compares the results of the EVP simulation, with the results of the EP simulations assuming isotropic (ISO) or kinematic (KINE) hardening, in terms of displacements, for the sensor C1, located under the fusion line, at the level of the first line support. It shows very little differences between the EVP and the EP simulation with isotropic hardening, both calculations giving satisfactory results.

Despite the EVP simulation is a little closer to the experiment, it seems that taking into account rate-dependant plasticity is not very significant on the results in terms of distortions. A purely elasto-plastic simulation assuming isotropic hardening seems to be sufficient to describe accurately the structural behavior of the plate, in this special case. This may be due to the fact that the identification of elasto-plastic data has been performed with deformation ratios similar to deformation ratios that are involved in this welding test.

The EP simulation with kinematic hardening, however, underestimates greatly the maximum of the transient displacement and also underestimates the final deflection of the center of the plate. The first vertical line in fig. 11 indicates the moment when the heat source is passing at the level of the sensor C1. The differences between kinematic and isotropic hardening can then only be seen from that moment. The second vertical line indicates the end of the welding. The effect of kinematic hardening is mainly visible during the welding. It is however difficult to conclude about the more realistic hypothesis for the hardening (isotropic or kinematic) as all the mechanical characterizations of the steel have been performed with tensile test only, without cyclic loading.

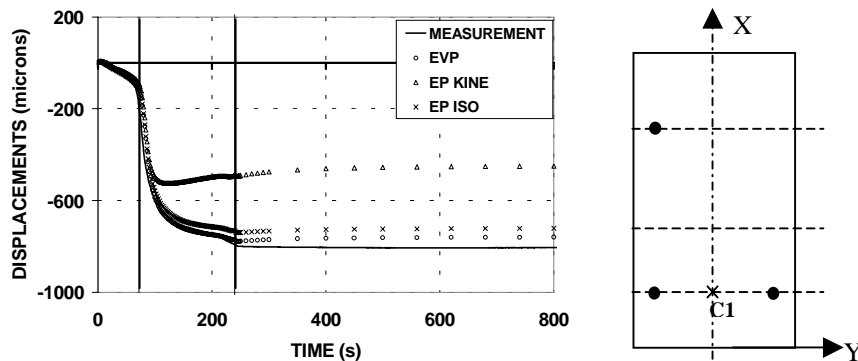


Figure 11. Evolution of transient vertical displacement of the sensor C1 during the test: comparison between EVP simulation, EP simulation with isotropic hardening, EP simulation with kinematic hardening, and measurements

3.5. Results – Residual stresses

Figs. 12 and 13 represent respectively the longitudinal residual stresses (in the direction of the weld), and the transverse residual stresses (orthogonal to the welding direction, in the lower face of a cross section). The measured residual stress field is mainly longitudinal, in the welding direction, with a typical pattern of tensile stresses near the weld and compressive stresses in the edges. Longitudinal stresses are between 200 to 300 MPa at the weld centerline, and drop to compressive values about 25 mm from the centerline, reaching approximately -200 MPa. The tensile transverse stresses are much lower, even in the center. Stresses measurements shows rises some questions, since a compressive transverse stress about -100 MPa has been measured at the edge of the plate, where the transverse stresses normally ought to be zero.

Apart from this uncertainty, measurements of both stress component σ_{xx} and σ_{yy} show a good symmetric pattern along the Y axis.

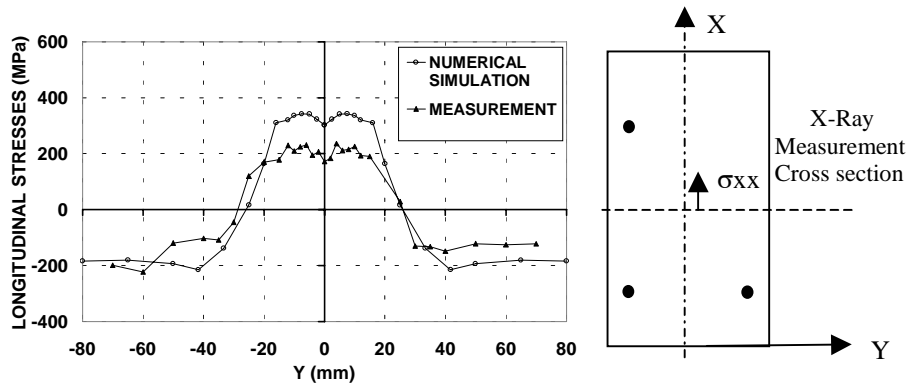


Figure 12. Longitudinal residual stresses in the lower face of a cross-section: comparison between EVP simulations and experimental measurements with X-Ray Diffraction

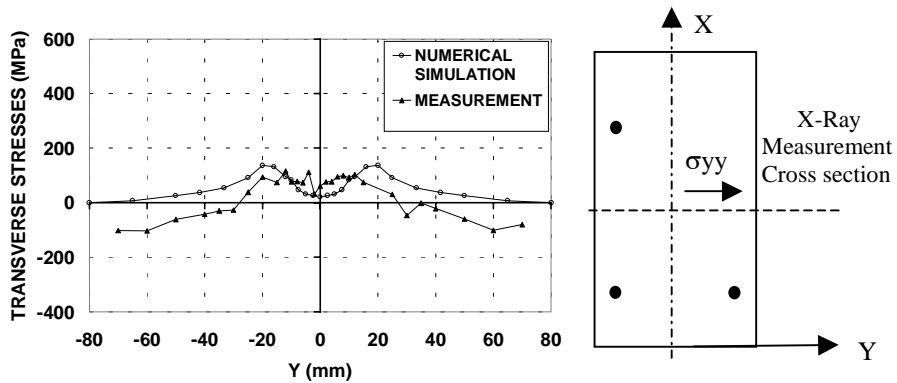


Figure 13. Transverse residual stresses in the lower face of a cross-section: comparison between EVP simulations and experimental measurements with X-Ray Diffraction

Fig. 12 and 13 compare experimental results with the solution of the EVP simulation, for the longitudinal and the transverse residual stresses, whereas fig. 14 compare the measured longitudinal stresses with results of the EP simulations, assuming one the one hand isotropic hardening, and on the other hand kinematic hardening. The calculated residual stresses are about the same in the lower and upper face of the plate for all the simulations.

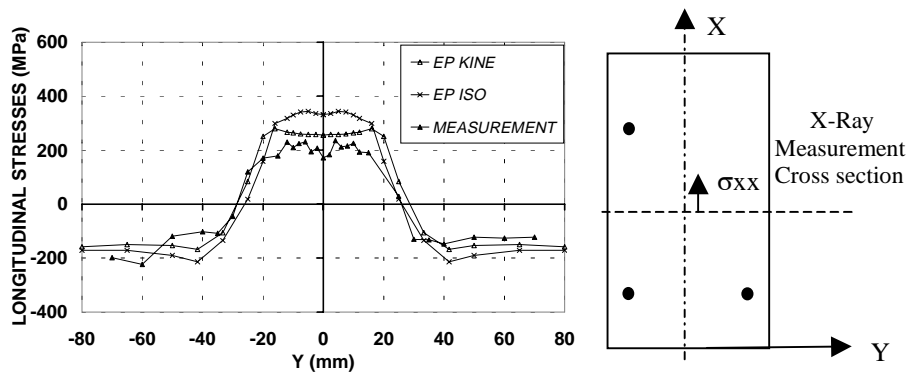


Figure 14. Longitudinal residual stresses in the lower face of a cross-section: comparison between experimental measurements with X-Ray Diffraction and EP simulations assuming isotropic or kinematic hardening

Comparison between fig. 12 and 14 shows that viscosity seems to have a negligible effect on the residual stress field in this special case, as EVP simulation and EP simulation with isotropic hardening give almost identical results.

Fig. 12 indicates a rather good agreement between the measured and calculated residual stresses with EVP modeling, except in the center, where the σ_{xx} component seems a little overestimated by the numerical simulation. This may be attributed to the fact that an isotropic hardening was assumed for the EVP calculation.

In fact, the comparison between EP simulation assuming isotropic hardening, and EP simulation assuming kinematic hardening, indicates a rather important difference of stresses level in the center of the plate. As reverse plasticity occurred during the cooling stage, kinematic hardening assumption led to a lower level of residual stresses in the center zone, and gave results closer to the experiment.

Nevertheless, kinematic hardening is less relevant for the prediction of transient displacements (fig. 11), although it is for the prediction of residual stresses. A possible explanation is that the hardening of the material may be mainly isotropic, but viscous recovery at high temperature can compensate the enlargement of the elastic domain, and lower the residual stresses level in the center. As viscous recovery is only taken into account for temperature exceeding 500°C in the EVP simulation, it might underestimate the lowering of the stresses during the cooling stage.

Except this discrepancy, numerical results are quite satisfactory as the stress evolution pattern with the Y axis is very well reproduced for all the simulations.

4. Two-dimensional finite element simulation

In this section, we consider simplified two-dimensional simulations, much faster and less computer demanding than the three-dimensional analysis. The aim is to compare the lost of accuracy involved by the choice of a 2D analysis, taking into consideration more interesting computational costs. Different kinds of 2D modeling can be assumed in this situation (Lindgren, 2001):

Two-dimensional simulations considering a cross-section, orthogonal to the welding direction, assuming a plane strain, or a generalized plane strain hypothesis (see for instance Anderson *et al.*, 1978, Grignon *et al.*, 2001, Michaleris *et al.*, 2001), are typically for common use for the simulation of multipasse welding, for which a 3-D analysis would demand too large computing power. However, the plane strain hypotheses is not satisfactory as it usually leads to an invalid representation of distortion, and to an overestimation of the longitudinal residual stress, parallel to the direction of welding (Mc Dill *et al.*, 1993).

More rarely performed, two-dimensional simulations assuming a plane stress hypothesis, are susceptible to give more satisfactory results in terms of residual stresses (Canas *et al.*, 1996).

Consequently, a 2D-plane stress model is considered here. This model ignores the stress in the thickness direction, and also ignores the temperature gradient through the thickness. Vertical displacements of the plate can not be computed in this model, as the deformation is assumed to be in the plane of the plate, but only residual stresses are for interest in this section.

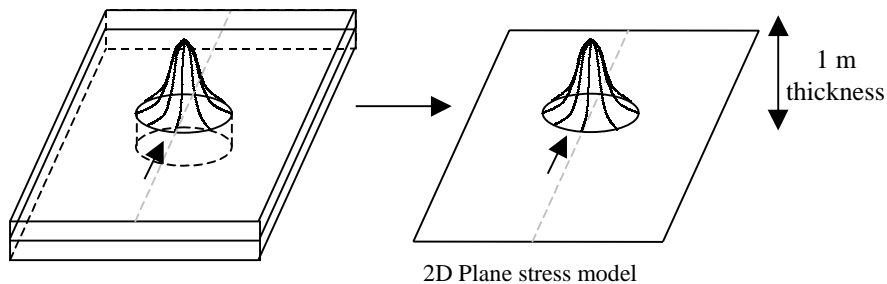


Figure 15. *2D plane-stress model*

Contrary to the plane strain model considering a weld cross-section, the plane stress model of the plate requires the discretization of the whole surface of the plate in its plane, in order to follow the volumetric heat source that moves in the plane of the mesh.

The mesh used for this 2D-plane stress model is similar to the mesh of the surface of the previous 3D model. It is quadratic, and consists in approximately 1300 nodes (only one half of the plate is modeled).

The same triangular heat source as for the 3D model is used. It was a surface heat flux density for the 3D model which was 10mm thick, whereas it is now a volumetric heat flux density, applied on the 2D mesh, considering one-meter thickness. The heat source for the 2D analysis is deduced in the following way:

$$\text{Heat flux (2D)} = \text{Heat flux (3D)} \times 1\text{m} / 0,01\text{m} \quad [8]$$

This heat flux density is moving along the axis direction. The temperature evolution of a point located under the heat source path can be considered as an average temperature evolution through the thickness of the 3D modeling.

The 2D plane-stress simulation is performed with the previously presented elasto-viscoplastic (EVP) constitutive equation (equations 4 to 7), and with the same temperature-dependent mechanical properties as used for the 3D analysis.

Fig. 16 compares residual longitudinal stresses obtained from the 3D modeling (in upper and in lower face) and from the 2D modeling, both simulation assuming an EVP constitutive equation. The 2D model gives very similar results to the 3D model for the longitudinal and transverse stress pattern along the weld line. In particular, the edge effects predicted by the 3D model (compressive stresses at the beginning and at the end of the weldline) is very similar for the 2D model.

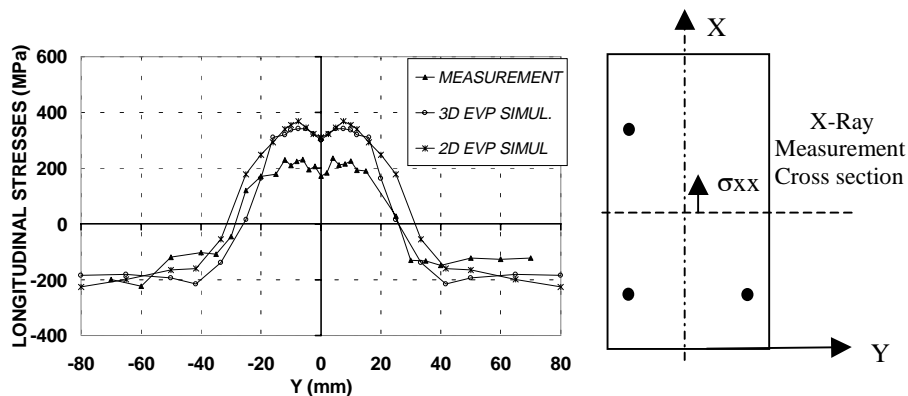


Figure 16. Comparison of longitudinal residual stresses obtained from 3D model and for 2D plane-stress mode, for the lower face of a cross-section

2D plane stress modeling is therefore a very interesting alternative to 3D modeling in order to investigate the stress evolution in the plate in such a test-case,

although it cannot reproduce transient displacements and final shape of the plate, as calculation times are divided by almost 80. It can also be useful for studying the stress evolution during the thermal cycle.

5. Conclusion

In this study, numerical simulations of a test case representative of a welding operation have been presented. The test case, which considers a moving TIG heat source along the axis of a 316L plate, provided a large quantities of measurement, and is then very useful to compare the predictions of different kinds of modeling. Firstly, 3D simulations of this test have been performed. For the thermal analysis, the net heat input was calibrated against temperature measurement. This calibration allowed us to reproduce very well the transient temperature field during the whole test. For the subsequent mechanical analysis, the viscosity effect was investigated, by comparing EVP simulation assuming isotropic hardening with recovery at high temperature, with EP simulations assuming on the one hand isotropic hardening, and on the other hand, kinematic hardening.

EVP simulations and EP simulation with isotropic hardening gave similar results, with a very good agreement with the experiment, in terms of transient displacements and final shape. The comparison between calculated and measured residual stresses is also satisfactory, but both EVP and EP simulation overestimate the tensile stress in the vicinity of the weld, which may be due to the assumption of isotropic hardening, but also to an underestimation of viscous recovery during the cooling stage. EP simulation with kinematic hardening predicts correct level of residual stresses, but underestimate the deflection of the plate.

Afterward, a comparison between 3D modeling and a 2D-plane stress modeling has revealed that the 2D plane stress simulation can be relevant in order to investigate the transient stress field and the residual stresses. This kind of 2D analysis is very much faster than the 3D analysis, and gives very similar results in terms of the residual stresses for this special test case. Nevertheless, all simulations required the calibration of the heat source against temperature measurements.

Acknowledgements

This numerical and experimental research has been supported by EDF, Framatome, and CEA.

6. Bibliography

Anderson B.A.B., "Thermal stresses in a submerged-arc welded joint considering phase transformations", *Journal of Engineering Materials and Technology*, Vol. 100, 1978, p. 356-362.

- Brickstad B., Josefson B.L., "A parametric study of residual stresses in multi-pass butt-welded stainless steel pipes", *International Journal of Pressure Vessels and Piping*, 75, 1998, p. 11-25.
- Bru D., Devaux J., Bergheau J.M., Pont D., "Influence of material properties at high temperatures on the modelling of welding residual stress and deformation state", *Mathematical Modelling of weld phenomena* 3, 1997, p. 456-463
- Canas J., Picon R., Paris F., Blazquez A., Marin J.C., "A simplified numerical analysis of residual stresses in aluminium welded plates", *Computers and Structures*, Vol. 58, No. 1, 1996, p. 59-69.
- Carmignani B., Tosselli G., Interlandi S., Lucca F., Marin A., "Numerical simulation of welds of thick steel sheets for some experimental models towards ITER TF coil case", *Fusion Engineering and Design*, 58-59, 2001, p. 231-236.
- Goldak J., Chakravati A., Bibby M., A new finite element model for welding heat sources, *Metallurgical Transactions*, 15B, 1984, p. 299-305
- Grignon C., Petitpas E., Perinet R., Condoure J., « Modélisation thermomécanique appliquée au soudage laser des aciers », *Int. J. Therm. Sci.*, 40, 2001, p. 669-680.
- Lindgren L.E., "Finite element modelling and simulation of welding, Part 1: increased complexity", *Journal of thermal stresses*, 24, 2001, p.141-192.
- Lindgren L.E., "Finite element modelling and simulation of welding, Part 2 : improved material modelling", *Journal of thermal stresses*, 24, 2001, p. 195-131.
- Mc Dill J.M.J., Oddy A.S., Goldak J.A., "Comparing 2-D plane strain and 3-D Analyses of residual stresses in welds", *Proceeding of the 3rd Int. Conf. on Trends in Welding Research*, 1993, p. 105-108.
- Michaleris P., Debicari A., "Prediction of welding distortion", *Welding Journal*, 76 (4), 1997, p. 172-180.
- Preston R.V., Shercliff H.R., Withers P.J., Smith S.D., "Finite element modelling of tungsten inert gas welding of aluminium alloy 2024", *Science and Technology of Welding and Joining*, Vol.8, No. 1, 2003, p. 10-18.
- Rosenthal D., "Mathematical theory of heat distribution during welding and cutting", *Welding Journal*, 20, 1941, p. 220s-234s.
- Shanghvi J., Michaleris P., "Thermo-elasto-plastic finite element analysis of quasi-state processes in eulerien reference frames", *Int. J. Numer. Meth. Eng.*, 53, 2002, p. 1533-1556.
- Tsirkas S.A., Papanikos P., Kermanidis T.H., "Numerical Simulation of the laser welding process in butt-joint specimens", *Journal of Materials Processing Technology*, 134, 2003, p. 59-69.
- Vincent Y., Bergheau J.M., Leblond J.B., "Viscoplastic behaviour of steels during phase transformations", *Comptes Rendus Mecanique*, 331, 2003, p. 587-594.
- Zhu, X.K., Chao, Y.J., "Effect of temperature-dependent material properties on welding simulation", *Computers and Structures*, 80, 2002, p. 967-976.